

Compressed Sensing with Invertible Generative Models and Dependent Noise

Jay Whang
jaywhang@cs.utexas.edu
University of Texas at Austin

Qi Lei
leiqi@ices.utexas.edu
University of Texas at Austin

Alexandros G. Dimakis
dimakis@austin.utexas.edu
University of Texas at Austin

Abstract

We study image inverse problems with invertible generative priors, specifically normalizing flow models. Our formulation views the solution as the Maximum a Posteriori (MAP) estimate of the image given the measurements. Our general formulation allows for non-linear differentiable forward operators and noise distributions with long-range dependencies. We establish theoretical recovery guarantees for denoising and compressed sensing under our framework. We also empirically validate our method on various inverse problems including compressed sensing with quantized measurements and denoising with dependent noise patterns.

1 Introduction

Inverse problems attempt to reconstruct an unknown signal, image or three dimensional volume from observations. We are interested in cases where the observations are obtained by a forward process which is non-invertible and hence there is loss of information. In such settings, the imaging algorithms critically rely on powerful prior knowledge to model the imaged data. Specifically, we would like to reconstruct \mathbf{x} by observing noisy measurements:

$$\mathbf{y} = f(\mathbf{x}) + \delta.$$

Here, \mathbf{y} are the observed measurements, f is a deterministic and known *forward operator* and δ is added noise which may also have a complex structure. The forward operator models a physical process that appears in e.g. magnetic resonance imaging (MRI) Lustig et al. [2007], compressed sensing Candes et al. [2006], Donoho [2006] or phase retrieval Candes et al. [2015a,b].

There is a vast literature on solving linear inverse problems where

$$\mathbf{y} = A\mathbf{x} + \delta,$$

for some measurement matrix A . Numerous useful problems fall under this category, including denoising, compressive sensing, super-resolution, and inpainting. Sparsity or structured sparsity Donoho [2006], Candes et al. [2006], Baraniuk et al. [2010] have been very influential structural priors used for inverse problems. More recently, deep generative models have been introduced as image priors Bora et al. [2017], Asim et al. [2019], Van Veen et al. [2018], showing significant performance benefits compared to sparsity priors.

Invertible deep generative models (also called normalizing flows) are a novel class of deep generative models that allow efficient sampling, inversion and likelihood estimation by construction [Papamakarios et al., 2019, and references therein]. Very recently Asim et al. [2019] showed that invertible models can



Figure 1: Denoising with MNIST noise. First column: Noisy Observations. Second Column: Reconstructions using our algorithm that leverages the structure of the signals and the noise. Third Column: Reconstructions using the method from Asim et al. [2019]. Fourth column: Reconstructions using the method from Bora et al. [2017]. Fifth column: Reconstructions using BM3D. We emphasize that the competing methods do not have knowledge about the structure of the noise and hence are at a disadvantage. Our method uses two invertible generative models, one for the noise and one for the signal. Our MAP framework combines the two models to separate MNIST digit noise from the reconstructed image.

yield significant performance improvements compared to GANs Bora et al. [2017], especially for imaging out-of-distribution samples. Inspired by this work, we extend the framework of Asim et al. [2019] to general noise distributions and differentiable forward operators.

Our contributions are as follows:

- We present a general formulation for obtaining maximum a priori (MAP) estimation reconstructions for dependent noise and general forward operators. For linear inverse problems and Gaussian noise, we retrieve the method of Asim et al. [2019].
- Our method can leverage invertible generative models for both the reconstructed image and the structured noise. For example we can handle noise with variable variance, or even dependent noise having a structure like MNIST digits.
- We show two theoretical results about the performance of our reconstruction method. The first is for the case of denoising: if the log-likelihood function of the generative model is strongly concave locally around the true image, we can show that gradient descent achieves a reduction in error that depends on the local convexity parameter. We further generalize the results of Bora et al. [2017] for compressive sensing with a random measurement matrix to bound the recovery error under our MAP formulation.
- Our experiments show excellent reconstruction in the presence of noise with various complex and dependent structures. We apply our method to CelebA-HQ and MNIST for various inverse problems including denoising and quantized compressive sensing.

2 Preliminaries

2.1 Invertible Generative Models

Invertible generative models, also known as *normalizing flow* models, approximate a complex distribution by mapping a simple noise (typically independent Gaussian) through a differentiable, invertible function G [Tabak and Turner, 2013]. Sampling is performed by first generating a noise vector \mathbf{z} from a simple distribution, and

computing $\mathbf{x} = G(\mathbf{z})$. Since G is invertible, change of variables formula allows us to compute the log-density of \mathbf{x} :

$$\log p(\mathbf{x}) = \log p(\mathbf{z}) + \log |\det J_{G^{-1}}(\mathbf{x})|, \quad (1)$$

where $J_{G^{-1}}(\mathbf{x})$ is the Jacobian of G^{-1} evaluated at \mathbf{x} . Since $\log p(\mathbf{z})$ is a simple distribution, computing the likelihood at any point \mathbf{x} is straightforward as long as G^{-1} and the log-determinant term can be efficiently evaluated.

Following the recent success of deep learning, numerous neural network architectures for G with tractable inverse and log-determinant computation have been proposed, including NICE [Dinh et al., 2014], RealNVP [Dinh et al., 2016], IAF [Kingma et al., 2016], iResNet [Behrmann et al., 2018], Glow [Kingma and Dhariwal, 2018], and FFJORD [Grathwohl et al., 2019].

We focus on *affine coupling layer* (ACL), which is the main building block for the models used in our experiments (RealNVP and Glow). ACL is an invertible neural network architecture whose Jacobian is triangular by construction, so that the determinant is simply the product of its diagonal entries. It works by splitting the input into two parts $x = (x_1, x_2) \in \mathbb{R}^{d_1} \times \mathbb{R}^{d_2}$. The output $y = (y_1, y_2)$ is computed as $y_1 = x_1, y_2 = s(x_1) \odot x_2 + t(x_1)$. This transformation can be easily inverted for arbitrary $s, t : \mathbb{R}^{d_1} \rightarrow \mathbb{R}^{d_2}$ via: $x_1 = y_1, x_2 = (y_2 - t(y_1))/s(y_1)$ (division is done elementwise). A simple calculation also shows that the log-determinant is simply $\sum_{i=1}^d \log s(y_1)_i$. By parametrizing s and t as deep neural networks (not necessarily invertible) and composing many such ACLs, one can build an invertible mapping that can express highly complex transformations while being able to efficiently compute the inverse and log-determinant.

2.2 Related Work

We briefly review existing literature on the application of deep generative models on inverse problems. While vast literature exists on compressive sensing and other inverse problems, the idea of using a deep generative prior was introduced relatively recently by Bora et al. [2017]. In that work, the generator from a GAN or a VAE [Goodfellow et al., 2014, Kingma and Welling, 2013] was shown to be an effective prior for compressive sensing. Several recent studies have investigated different ways to incorporate deep generative models into inverse problems. In [Dhar et al., 2018], an extension to [Bora et al., 2017] was proposed by allowing sparse deviations from the range of the generator. Van Veen et al. [2018] showed that an *untrained* convolutional neural network can be used as a prior for imaging tasks based on Deep Image Prior by Ulyanov et al. [2018]. More recently, Wu et al. [2019] applied techniques from meta-learning to improve the reconstruction speed, and Ardizzone et al. [2018] showed that by modelling the forward process with a flow model, one can *implicitly* learn the inverse process through the invertibility of the model. Asim et al. [2019] proposed to replace the GAN prior of [Bora et al., 2017] with a normalizing flow model and reported excellent generalization performance, especially on reconstructions of out-of-distribution images.

3 Methodology

3.1 Notation and Setup

We use bold lower-case variables to denote vectors and use $\|\cdot\|$ to denote ℓ_2 norm for vectors unless otherwise specified. Also \odot denotes element-wise multiplication. We assume the existence of an (unknown) true data distribution $p(\mathbf{x})$, a deterministic, differentiable forward operator f , and a noise density $p_\Delta(\delta)$. An observation is generated via

$$\mathbf{y} = f(\mathbf{x}) + \delta$$

where $\mathbf{x} \sim p$ and $\delta \sim p_\Delta$.

3.2 MAP Formulation

For a given observation \mathbf{y} , our method tries to recover \mathbf{x} as the minimizer of the following loss:

$$L_{\text{MAP}}(\mathbf{x}; \mathbf{y}) \triangleq -\log p_{\Delta}(\mathbf{y} - f(\mathbf{x})) - \log p(\mathbf{x}) \quad (2)$$

We now show that the minimizer of this loss is the Maximum a Posteriori (MAP) estimate of the the posterior $p(\mathbf{x}|\mathbf{y})$.

$$\begin{aligned} \bar{\mathbf{x}} &\stackrel{(1)}{=} \arg \max_{\mathbf{x}} p(\mathbf{x}|\mathbf{y}) = \arg \max_{\mathbf{x}} \log p(\mathbf{x}|\mathbf{y}) \\ &\stackrel{(2)}{=} \arg \max_{\mathbf{x}} [\log p(\mathbf{y}|\mathbf{x}) + \log p(\mathbf{x}) - \log p(\mathbf{y})] \\ &\stackrel{(3)}{=} \arg \max_{\mathbf{x}} [\log p(\boldsymbol{\delta} = \mathbf{y} - f(\mathbf{x})) + \log p(\mathbf{x}) - \log p(\mathbf{y})] \\ &\stackrel{(4)}{=} \arg \max_{\mathbf{x}} [\log p(\boldsymbol{\delta} = \mathbf{y} - f(\mathbf{x})) + \log p(\mathbf{x})] \\ &\stackrel{(5)}{=} \arg \max_{\mathbf{x}} [\log p_{\Delta}(\mathbf{y} - f(\mathbf{x})) + \log p(\mathbf{x})] \\ &= \arg \min_{\mathbf{x}} L_{\text{MAP}}(\mathbf{x}; \mathbf{y}) \end{aligned}$$

Note that (1) follows from the monotonicity of \log , (2) follows from Bayes Rule $p(\mathbf{x}|\mathbf{y}) = \frac{p(\mathbf{y}|\mathbf{x}) \cdot p(\mathbf{x})}{p(\mathbf{y})}$, and (3) follows from $\boldsymbol{\delta} = \mathbf{y} - f(\mathbf{x})$. In (4) we drop the marginal density $\log p(\mathbf{y})$ since it is a constant, and in (5) we simply rewrite the first term as the log-density of noise.

Now suppose we have a flow model $p_G(\mathbf{x})$ that models $p(\mathbf{x})$, defined by an invertible mapping G . If $p_G(\mathbf{x})$ is perfect, then we can replace $p(\mathbf{x})$ with it: $L_{\text{MAP}}(\mathbf{x}; \mathbf{y}) = -\log p_{\Delta}(\mathbf{y} - f(\mathbf{x})) - \log p_G(\mathbf{x})$. Recalling that the sampling procedure for the flow model is $\mathbf{z} \sim \mathcal{N}(\mathbf{0}, I_d)$, $\mathbf{x} = G(\mathbf{z})$, we arrive at the following loss function:

$$L_G(\mathbf{z}; \mathbf{y}) \triangleq -\log p_{\Delta}(\mathbf{y} - f(G(\mathbf{z}))) - \log p_G(G(\mathbf{z})) \quad (3)$$

Note that the invertibility of G allows us to minimize the above loss in two different ways:

$$\begin{aligned} \arg \min_{\mathbf{z}} L_G(\mathbf{z}; \mathbf{y}) &= \arg \min_{\mathbf{z}} [-\log p_{\Delta}(\mathbf{y} - f(G(\mathbf{z}))) - \log p_G(G(\mathbf{z}))] \\ &= \arg \min_{\mathbf{x}} [-\log p_{\Delta}(\mathbf{y} - f(\mathbf{x})) - \log p_G(\mathbf{x})] \\ &= \arg \min_{\mathbf{x}} L_G(\mathbf{x}; \mathbf{y}) \end{aligned}$$

Since the above optimization objective non-convex but differentiable, any gradient-based optimizer can be used to approximately find the minimizer. In practice, even with an imperfect model and approximate optimization, we observe that our approach performs well across a wide range of tasks.

3.3 Connection to Prior Work

This paper builds upon the work of Bora et al. [2017] and Asim et al. [2019], so we describe the loss functions used in those papers in detail.

3.3.1 GAN Prior

Bora et al. [2017] consider the following loss:

$$L_{\text{Bora}}(\mathbf{z}; \mathbf{y}) = \|\mathbf{y} - f(G(\mathbf{z}))\|^2 + \lambda \|\mathbf{z}\|^2, \quad (4)$$

which tries to project the input \mathbf{y} onto the range of the generator G with ℓ_2 regularization on the latent variable. While it looks similar to our loss, this approach is conceptually very different. First, the generator G here is not invertible as it maps a noise to a higher-dimensional vector. This means that the ground truth image we wish to recover may not be in the range of G . The inability to represent any arbitrary input was pointed out by Asim et al. [2019] as well, and this does lead to poor reconstruction as our experiments show. Also this formulation does not offer a probabilistic interpretation because GANs generally do not provide likelihood.

3.3.2 Flow Prior

[Asim et al., 2019] has been the main inspiration for our work. In that paper the authors consider an objective similar to ours that tries to simultaneously match the observation and maximize the likelihood:

$$L(\mathbf{z}; \mathbf{y}) = \|\mathbf{y} - f(G(\mathbf{z}))\|^2 - \gamma \log p_G(\mathbf{x}), \quad (5)$$

for some hyperparameter $\gamma > 0$. When the noise is isotropic Gaussian $\delta \sim \mathcal{N}(\mathbf{0}, \gamma I_d)$ our loss obtains the form introduced by Asim et al. [2019]. Because the log-density of δ in this case is $\log p_\Delta(\delta) = -\frac{1}{2\gamma} \|\delta\|^2 - C$ for some constant C , our loss reduces to

$$\arg \min_{\mathbf{z}} L_G(\mathbf{z}; \mathbf{y}) = \arg \min_{\mathbf{z}} -\log p_\Delta(\mathbf{y} - f(\mathbf{z})) - \log p_G(G(\mathbf{z})) \quad (6)$$

$$= \arg \min_{\mathbf{z}} \frac{1}{2\gamma} \|\mathbf{y} - f(G(\mathbf{z}))\|^2 - \log p_G(G(\mathbf{z})) \quad (7)$$

$$= \arg \min_{\mathbf{z}} \|\mathbf{y} - f(G(\mathbf{z}))\|^2 - \gamma \log p_G(G(\mathbf{z})). \quad (8)$$

Asim et al. [2019] also report that due to optimization difficulty, they use the following proxy loss:

$$L_{\text{Asim}}(\mathbf{z}; \mathbf{y}) = \|\mathbf{y} - f(G(\mathbf{z}))\|^2 + \gamma \|\mathbf{z}\|. \quad (9)$$

We note that this loss is also closely related to a specific instance of our loss. To see this, again suppose that noise δ is isotropic Gaussian $\mathcal{N}(\mathbf{0}, \gamma I_d)$ and that the flow prior is volume-preserving up to a constant shift, i.e. the log-determinant term is constant. Thus by the change of variables formula from eq. (1), we have

$$\begin{aligned} \log p_G(\mathbf{x}) &= \log \underbrace{p(\mathbf{z})}_{\propto \exp(-\|\mathbf{z}\|^2)} + \underbrace{\log |\det J_{G^{-1}}(\mathbf{x})|}_{\text{constant}} \\ &= -\|\mathbf{z}\|^2 + C \end{aligned}$$

for some constant C . Then our loss reduces to the ℓ_2 -regularized version of L_{Asim} as shown below. Continuing from eq. (8):

$$\begin{aligned} \arg \min_{\mathbf{z}} L_G(\mathbf{z}; \mathbf{y}) &= \arg \min_{\mathbf{z}} \|\mathbf{y} - f(G(\mathbf{z}))\|^2 - \gamma \log p_G(G(\mathbf{z})) \\ &= \arg \min_{\mathbf{z}} \|\mathbf{y} - f(G(\mathbf{z}))\|^2 - \gamma (-\|\mathbf{z}\|^2 + C) \\ &= \arg \min_{\mathbf{z}} \|\mathbf{y} - f(G(\mathbf{z}))\|^2 + \gamma \|\mathbf{z}\|^2 \end{aligned}$$

Architectures that have the volume-preserving property include NICE Dinh et al. [2014] and Glow Kingma and Dhariwal [2018] with additive coupling layer.

4 Theoretical Analysis

In this section we provide some theoretical analysis for the proposed MAP inference. Unlike most prior work, we do not assume specific structures on the signal we want to recover, such as sparsity or being generated from a low-dimensional Gaussian prior. Instead, we consider a general setting and investigate how a pre-trained flow model could help reduce the recovery error in denoising problems, or reduce the number of measurements required in the context of compressed sensing.

4.1 Recovery Guarantees for Denoising problems

We consider the setting where we observe $\mathbf{y} = \mathbf{x}^* + \delta$ and the noise is $\delta \sim p_\Delta = \mathcal{N}(0, \sigma^2 I)$. Then we perform the MAP inference by minimizing the loss

$$L(\mathbf{x}) = q(\mathbf{x}) + \frac{1}{2\sigma^2} \|\mathbf{x} - \mathbf{y}\|^2, \quad (10)$$

where $q(\mathbf{x}) \triangleq -\log p(\mathbf{x})$. Notice we want to recover the natural images with high probability under our flow model instead of an arbitrary point. Thus we consider the case where the ground truth image \mathbf{x}^* is a local maximum of p .

Theorem 4.1. *Let \mathbf{x}^* be a local optimum of our learned model $p(\mathbf{x})$. Let $\mathbf{y} = \mathbf{x}^* + \delta$ be the noisy observation. Assume there is a neighborhood of \mathbf{x}^* defined as $B_r^d(\mathbf{x}^*) \triangleq \{\mathbf{x} \in \mathbb{R}^d : \|\mathbf{x} - \mathbf{x}^*\| \leq r\}$ such that q satisfies local strong convexity, i.e. the Hessian of q satisfies $H_q(\mathbf{x}) \succeq \mu I$ for some $\mu > 0$ and $\forall \mathbf{x} \in B_r^d(\mathbf{x}^*)$. If the noise is bounded (i.e. $\|\delta\| \leq r$), then gradient descent with initial point \mathbf{y} on the loss function (10) converges to $\bar{\mathbf{x}}$, a local minimizer of $L(\mathbf{x})$ that satisfies:*

$$\|\bar{\mathbf{x}} - \mathbf{x}^*\| \leq \frac{1}{\mu\sigma^2 + 1} \|\delta\| < \|\delta\|.$$

This result shows that desirable local properties such as strong-convexity improve the quality of our recovery. In other words, a well-conditioned model with large μ leads to better denoising. It suggests that our MAP formulation encourages reconstructions with high probability density. Thus, the maximum-likelihood training objective is in fact aligned with better denoising performance.

4.2 Recovery Guarantees for Compressed Sensing

Here we show a worst-case bound for noisy compressed sensing where we observe $\mathbf{y} = A\mathbf{x}^* + \delta$. Note that the following constrained minimization problem is equivalent to the original unconstrained minimization of the loss in eq. (12) for a particular β via Lagrange multipliers.

Theorem 4.2. *For a given \mathbf{x}^* and $q = \log p(\mathbf{x}^*)$, define $S(q) = \{\mathbf{x} | \log p(\mathbf{x}) \geq q\}$. Recall that the observation for \mathbf{x}^* is $\mathbf{y} = A\mathbf{x}^* + \delta$ where $A \in \mathbb{R}^{m \times d}$ has entries drawn i.i.d. from $\mathcal{N}(0, 1/m)$ and the noise level is $\epsilon = \|\delta\|_2$. When we perform the MAP inference by solving the following optimization problem,*

$$\bar{\mathbf{x}} \leftarrow \arg \min_{\mathbf{x} \in \mathbb{R}^d, \|A\mathbf{x} - \mathbf{y}\|_2 \leq \epsilon} \{-\log p(\mathbf{x})\}, \quad (11)$$

we have:

$$\mathbb{E} \|\bar{\mathbf{x}} - \mathbf{x}^*\|_2 \leq \sqrt{8\pi} \left(\frac{w(S(q))}{\sqrt{m}} + \epsilon \right),$$

where $w(K)$ is the Gaussian mean width of the set K .

Here $S(q) = \{\mathbf{x} | \log p(\mathbf{x}) \geq q\}$ is the set of images with probability density higher than the ground truth image. The expectation is over the randomness of A .

We note that in high dimensions, Gaussian mean width is on the same order as the size (i.e. the Lebesgue measure) of the set. Since the set $S(q)$ becomes smaller as q increases, this means the above error bound is tighter for ground truth images \mathbf{x}^* with high density. In the extreme case where \mathbf{x}^* is the global maximum of the density function, we achieve zero recovery error.

5 Experiments

Our experiments are designed to test how well our MAP formulation performs in practice as we deviate from the commonly studied setting of linear inverse problems in small dimensions. Specifically, we consider the following three cases: (1) non-linear forward operator, (2) complex noise with dependency, and (3) scalability to high dimensions.

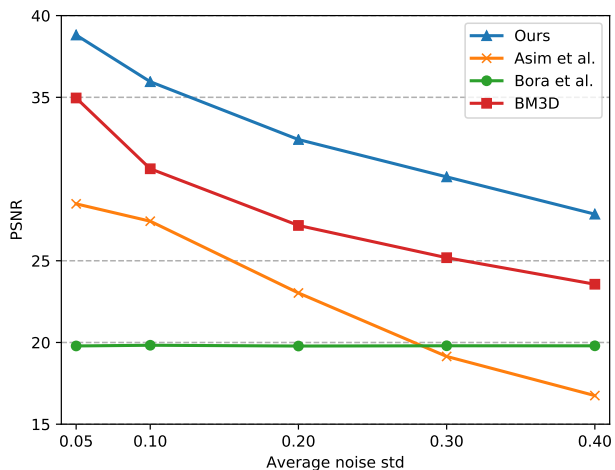


Figure 2: Result of denoising SINUSOIDAL noise on examples from CelebA-HQ test set at varying noise rates. As it can be seen, the proposed method achieves the same reconstruction performance even when the noise has approximately $3\times$ higher average standard deviation, corresponding to $9\times$ higher noise power compared to the best baseline method which is BM3D for this setting.

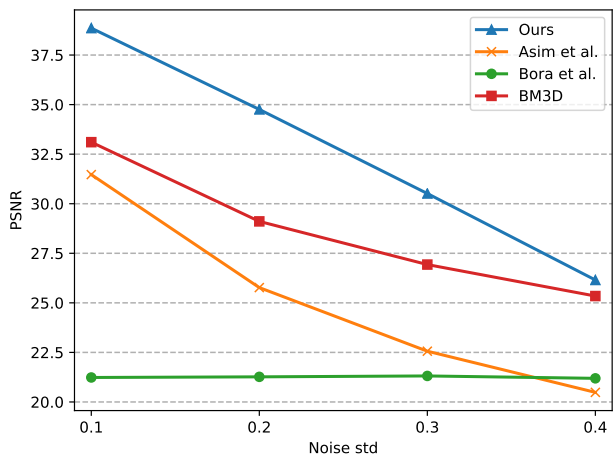


Figure 3: Result of denoising RADIAL noise on examples from CelebA-HQ test set at varying noise rates. As it can be seen, the proposed method achieves the same reconstruction performance even when the noise has approximately $1.5\times$ higher average standard deviation, corresponding to $2.2\times$ higher noise power compared to the best baseline method which is BM3D for this setting.

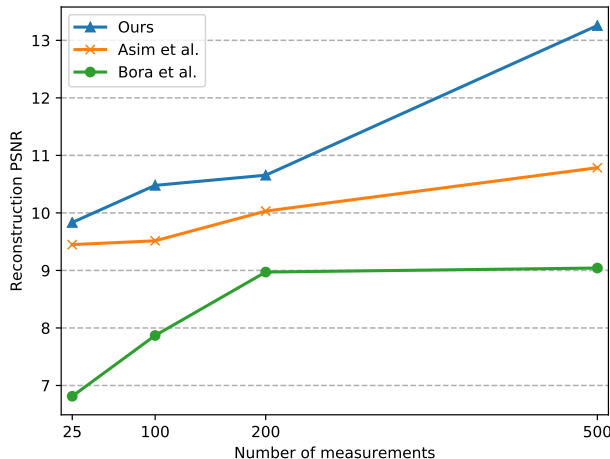


Figure 4: Result of 1-bit compressed sensing reconstructions as the number of measurements varies. As it can be seen, the proposed method achieves the same reconstruction performance using approximately $2\times$ fewer measurements compared to the best baseline method which is Asim et al. [2019] for this setting.

5.1 Datasets and Architecture

We trained multiscale RealNVP models on two standard image datasets MNIST and CelebA-HQ LeCun et al. [1998], Liu et al. [2015]. The MNIST model was trained on 60,000 training images normalized to $[0, 1]$. The CelebA-HQ model was trained on 27,000 training images resized to 64×64 , also normalized to $[0, 1]$. A detailed description of these models is provided in Appendix C.

We also use the publicly-available¹ Glow model released by Kingma and Dhariwal [2018] trained on 256×256 CelebA-HQ images. Due to computational constraints, our evaluations were done on 100 randomly-selected² images (1000 for MNIST) from the CelebA-HQ test set.

Lastly, we also augment our datasets with out-of-distribution images (see Figure 5).



Figure 5: Out-of-distribution images used in our experiments. We included different types of out-of-distribution instances including greyscale images and cartoons with flat image areas.

5.2 Baseline Methods

We compare our approach to the methods of [Bora et al., 2017] and [Asim et al., 2019], as they are two recently proposed approaches that use deep generative prior on inverse problems. In addition, we also compare against BM3D [Dabov et al., 2006], a popular off-the-shelf image denoising algorithm, whenever applicable. Note that for the 1-bit compressed sensing experiment, many existing techniques such as LASSO Tibshirani [1996] do not apply, since our task involves quantization as well as non-Gaussian noise. For more detailed experiment setup including hyperparameters, please refer to the Appendix.

¹Available at <https://github.com/openai/glow>.

²Indices were generated using the following Python script:

```
np.random.seed(0)
indices=np.random.choice(3000,100,False)
```


5.3 Model Smoothing Parameter

Recall that in our derivation of the loss function eq. (3), the unknown true data distribution $p(\mathbf{x})$ was approximated by the density given by a flow model $p_G(\mathbf{x})$. Thus our recovery of \mathbf{x} depends heavily on the quality of density estimates from $p_G(\mathbf{x})$.

It is well-known that likelihood-based models exhibit counter-intuitive properties, such as assigning high density on out-of-distribution examples or constant input Nalisnick et al. [2018], Choi et al. [2018], Hendrycks and Dietterich [2018], Nalisnick et al. [2019]. We empirically observe such behavior from our models as well.

To remedy this, we replace our model density by the smoothed version $p_G(x)^\beta$ where $\beta \geq 0$ is the *smoothing parameter*. Since the two extremes $\beta = 0$ and $\beta = \infty$ reduce to only using the noise density and the model density, respectively, β controls the degree to which we rely on p_G . Thus the loss we minimize becomes

$$L_G(\mathbf{z}; \mathbf{y}, \beta) = -\log p_\Delta(\mathbf{y} - f(G(\mathbf{z}))) - \beta \log p_G(G(\mathbf{z})) \quad (12)$$

5.4 Results

5.4.1 Removing MNIST Noise

We consider the measurement process $\mathbf{y} = 0.5 \cdot \mathbf{x} + \delta_{\text{MNIST}}$, where the added noise δ_{MNIST} contains multiple handwritten digits in different locations and color channels. Each digit is generated by another flow model trained on the MNIST dataset. Because \mathbf{x} and δ are both images added to each other, this can be viewed as an image decomposition problem where we try to separate two images from their “sum”. Note that the scaling factor 0.5 for \mathbf{x} is there purely for visualization purpose to make the noise more easily distinguished from the background.

As shown in Figure 6, our method can successfully remove MNIST noise while other baselines fail to do so. Notably the method by Bora et al. [2017] also removes the MNIST digits since all reconstructed images are in the range of DCGAN and hence are forced to look like faces.

5.4.2 Removing SINUSOIDAL Noise

We consider the measurement process $\mathbf{y} = \mathbf{x} + \delta_{\text{sine}}$, where the noise in each row follows a Gaussian distribution with variance that follows a sinusoidal pattern. The standard deviation for the pixels in the k -th row is computed as $\sigma(k) \propto \exp\left(\frac{2\pi k}{16}\right)$ normalized to have the maximum variance of 1.

See Figure 7 for the samples of recovered images.

5.4.3 Removing RADIAL Noise

We consider the measurement process $\mathbf{y} = \mathbf{x} + \delta_{\text{radial}}$, where each pixel again follows a Gaussian distribution, but with variance that decays exponentially in distance to the center point. For a pixel whose ℓ_2 distance to the center pixel is d , the standard deviation is computed as $\sigma(d) = \exp(-0.005 \cdot d^2)$.

See Figure 8 for the samples of recovered images.

5.4.4 Noisy 1-bit Compressive Sensing

This task considers a combination of a non-linear forward operator as well as a non-Gaussian noise. The measurement process is $\mathbf{y} = \text{sign}(A\mathbf{x}) + \delta_{\text{sine}}$ where $A \in \mathbb{R}^{m \times d}$ is random Gaussian measurement matrix ($A_{ij} \sim \mathcal{N}(0, \frac{1}{m})$). The noise is a 1-dimensional version of the sinusoidal noise from above, with a constant shift so that the mean is positive for all dimensions.

This is the most extreme case of quantized compressive sensing, where the observation only contains the noisy version of the sign $\{+1, -1\}$ of the measurements. Because the measurement $\text{sign}(A\mathbf{x})$ is a binary vector in $\{-1, +1\}^m$, having positive-mean noise causes more signs to be flipped from negative to positive than the other way around. This asymmetry is a challenge to algorithms that assume zero-mean noise.

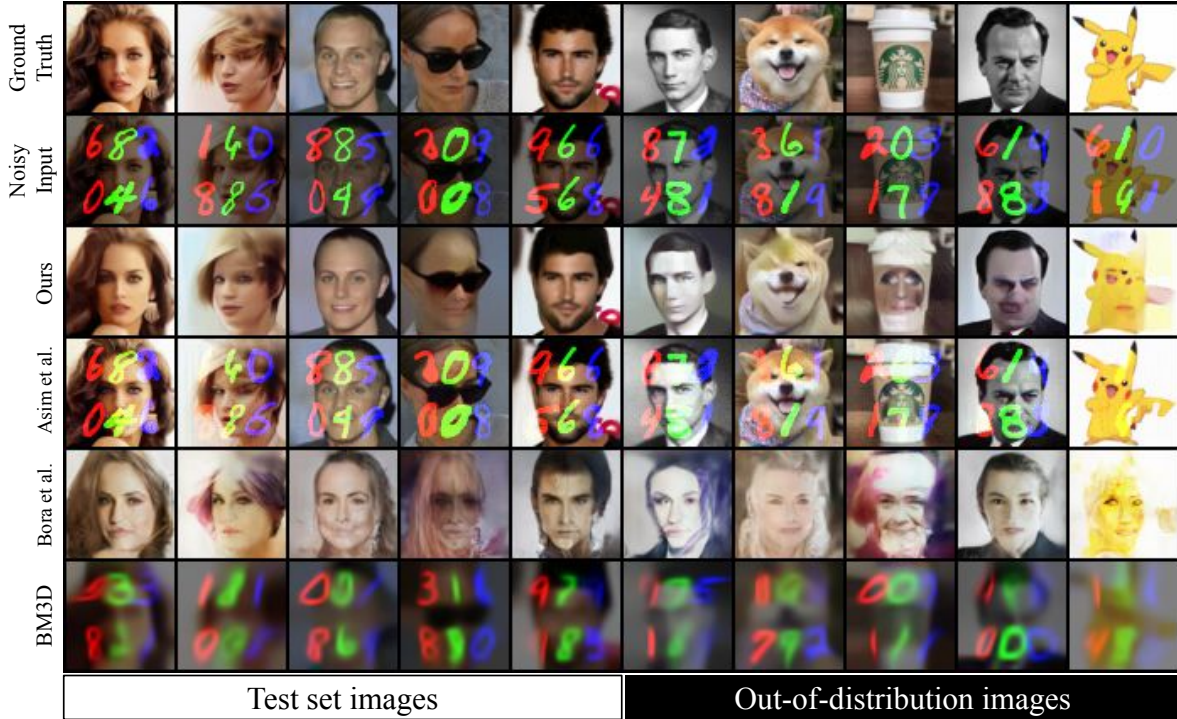


Figure 6: Result of denoising MNIST digits overlaid on top of CelebA-HQ faces. Notice that without any understanding of the complex noise structure, baseline methods fail to remove the digits.

Because the gradient of sign function is zero everywhere, we use Straight-Through Estimator Bengio et al. [2013] for backpropagation.

See Figure 4 for a comparison of our method to the baselines for varying numbers of measurements.

5.4.5 Sub-pixel Imputation

This task considers the measurement process $\mathbf{y} = M \odot \mathbf{x}$, where M is a random binary mask with each entry sampled from $\text{Ber}(0.75)$. In other words, we randomly drop 25% of the sub-pixels and try to fill them in. While the task is linear and noiseless, we note that this experiment aims to show the speed and scalability of our method – by running it on 256×256 images with a state-of-the-art pretrained Glow model instead of RealNVP. The high quality reconstructions in Figure 9 confirm that our approach is agnostic to the particular flow architecture and scales to high-dimensional setting in terms of both recovery quality and run time.

6 Conclusion

We proposed a novel method to solve inverse problems for general differentiable forward operators and structured noise. We emphasize again that the comparisons to baselines are not fair since our method knows the noise structure while other methods have not been designed to solve such general problems.

Our method can be seen as an extension of Asim et al. [2019] to more general forward operators and noise models. The power of our approach stems from the flexibility of invertible generative models which can be combined in a modular way to solve MAP inverse problems in very general settings, as we demonstrate. The central theoretical question that remains open is to analyze the optimization problem we formulated. In this paper we empirically minimize this loss using gradient descent but some theoretical guarantees would be very interesting, possibly under assumptions, e.g. random weights following the framework of Hand and Voroninski [2020].

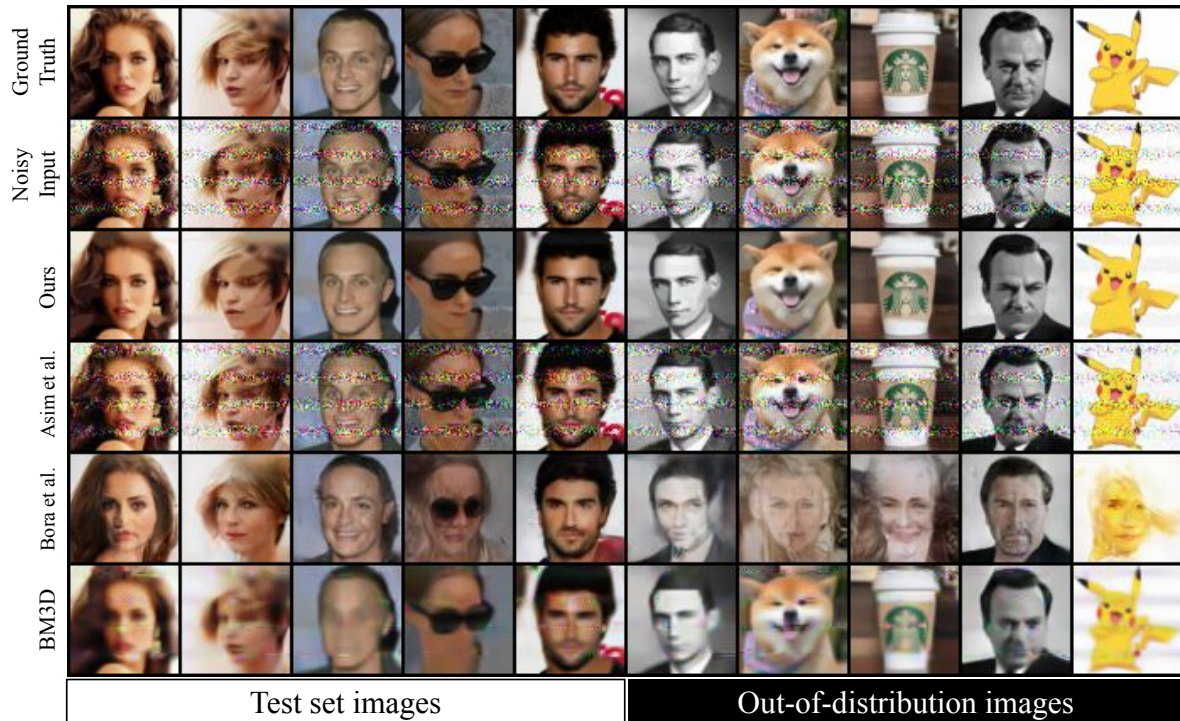


Figure 7: Result of denoising SINUSOIDAL noise on CelebA-HQ faces and out-of-distribution images. Notice that the method of [Bora et al., 2017], due to its limited representational power, attempts to find faces that resemble out-of-distribution images that are not human faces.

Acknowledgements

This research has been supported by NSF Grants 1618689, DMS 1723052, CCF 1763702, AF 1901292 and research gifts by Google, Western Digital and NVIDIA.

References

- Michael Lustig, David Donoho, and John M Pauly. Sparse mri: The application of compressed sensing for rapid mr imaging. *Magnetic Resonance in Medicine: An Official Journal of the International Society for Magnetic Resonance in Medicine*, 58(6):1182–1195, 2007.
- Emmanuel J Candes, Justin K Romberg, and Terence Tao. Stable signal recovery from incomplete and inaccurate measurements. *Communications on pure and applied mathematics*, 59(8):1207–1223, 2006.
- David L Donoho. Compressed sensing. *IEEE Transactions on information theory*, 52(4):1289–1306, 2006.
- Emmanuel J Candes, Yonina C Eldar, Thomas Strohmer, and Vladislav Voroninski. Phase retrieval via matrix completion. *SIAM review*, 57(2):225–251, 2015a.
- Emmanuel J Candes, Xiaodong Li, and Mahdi Soltanolkotabi. Phase retrieval via wirtinger flow: Theory and algorithms. *IEEE Transactions on Information Theory*, 61(4):1985–2007, 2015b.
- Muhammad Asim, Ali Ahmed, and Paul Hand. Invertible generative models for inverse problems: mitigating representation error and dataset bias. *CoRR*, abs/1905.11672, 2019. URL <http://arxiv.org/abs/1905.11672>.

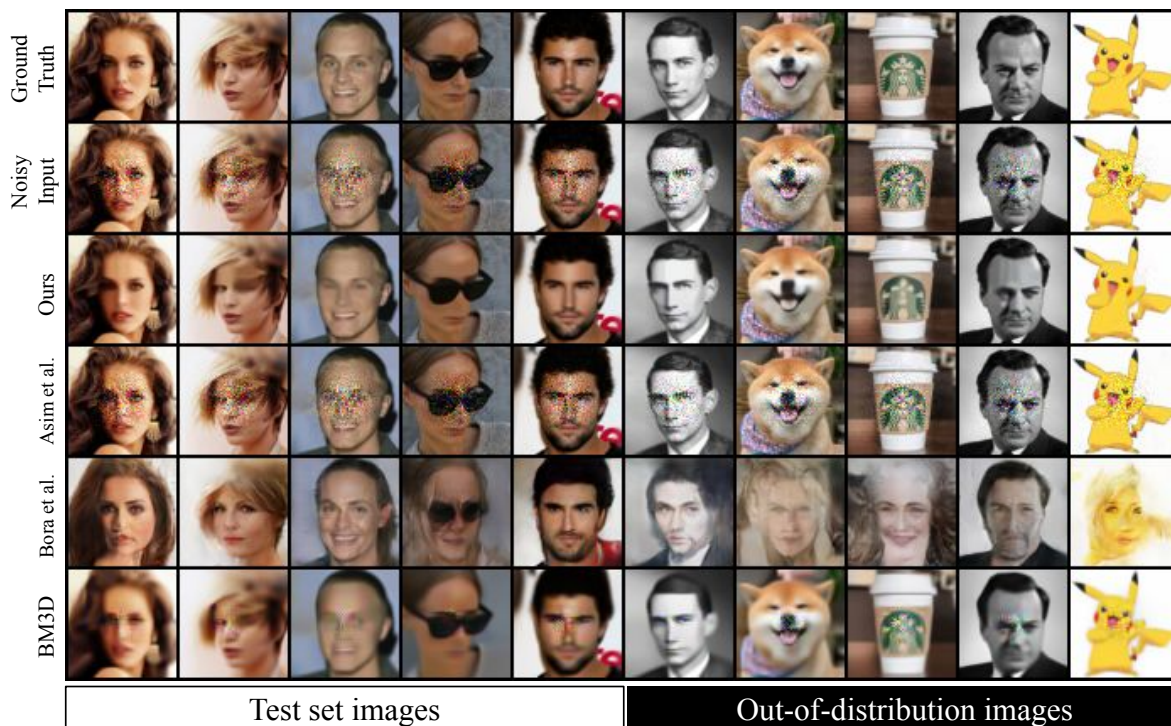


Figure 8: Result of denoising RADIAL noise on CelebA-HQ faces and out-of-distribution images.



Figure 9: Scalability to higher resolutions. We show denoising progress of sub-pixel imputation at 256×256 resolution. Note that the recovery takes less than 20 minutes on one NVidia GTX 1080 Ti for a batch of 2 images. In comparison, Asim et al. [2019] report that their method takes 15 minutes for a batch of 6 images at 64×64 resolution.

Ashish Bora, Ajil Jalal, Eric Price, and Alexandros G Dimakis. Compressed sensing using generative models. In *Proceedings of the 34th International Conference on Machine Learning-Volume 70*, pages 537–546. JMLR. org, 2017.

- Richard G Baraniuk, Volkan Cevher, Marco F Duarte, and Chinmay Hegde. Model-based compressive sensing. *IEEE Transactions on information theory*, 56(4):1982–2001, 2010.
- Dave Van Veen, Ajil Jalal, Mahdi Soltanolkotabi, Eric Price, Sriram Vishwanath, and Alexandros G Dimakis. Compressed sensing with deep image prior and learned regularization. *arXiv preprint arXiv:1806.06438*, 2018.
- George Papamakarios, Eric Nalisnick, Danilo Jimenez Rezende, Shakir Mohamed, and Balaji Lakshminarayanan. Normalizing flows for probabilistic modeling and inference. *arXiv preprint arXiv:1912.02762*, 2019.
- Esteban G Tabak and Cristina V Turner. A family of nonparametric density estimation algorithms. *Communications on Pure and Applied Mathematics*, 66(2):145–164, 2013.
- Laurent Dinh, David Krueger, and Yoshua Bengio. Nice: Non-linear independent components estimation. *arXiv preprint arXiv:1410.8516*, 2014.
- Laurent Dinh, Jascha Sohl-Dickstein, and Samy Bengio. Density estimation using real nvp. *arXiv preprint arXiv:1605.08803*, 2016.
- Durk P Kingma, Tim Salimans, Rafal Jozefowicz, Xi Chen, Ilya Sutskever, and Max Welling. Improved variational inference with inverse autoregressive flow. In *Advances in neural information processing systems*, pages 4743–4751, 2016.
- Jens Behrmann, Will Grathwohl, Ricky TQ Chen, David Duvenaud, and Jörn-Henrik Jacobsen. Invertible residual networks. *arXiv preprint arXiv:1811.00995*, 2018.
- Durk P Kingma and Prafulla Dhariwal. Glow: Generative flow with invertible 1x1 convolutions. In *Advances in Neural Information Processing Systems*, pages 10215–10224, 2018.
- Will Grathwohl, Ricky TQ Chen, Jesse Bettencourt, Ilya Sutskever, and David Duvenaud. Fjord: Free-form continuous dynamics for scalable reversible generative models. *arXiv preprint arXiv:1810.01367*, pages 6–9, 2019.
- Ian Goodfellow, Jean Pouget-Abadie, Mehdi Mirza, Bing Xu, David Warde-Farley, Sherjil Ozair, Aaron Courville, and Yoshua Bengio. Generative adversarial nets. In *Advances in neural information processing systems*, pages 2672–2680, 2014.
- Diederik P Kingma and Max Welling. Auto-encoding variational bayes. *arXiv preprint arXiv:1312.6114*, 2013.
- Manik Dhar, Aditya Grover, and Stefano Ermon. Modeling sparse deviations for compressed sensing using generative models, 2018.
- Dmitry Ulyanov, Andrea Vedaldi, and Victor Lempitsky. Deep image prior. In *Proceedings of the IEEE Conference on Computer Vision and Pattern Recognition*, pages 9446–9454, 2018.
- Yan Wu, Mihaela Rosca, and Timothy P. Lillicrap. Deep compressed sensing. *CoRR*, abs/1905.06723, 2019. URL <http://arxiv.org/abs/1905.06723>.
- Lynton Ardizzone, Jakob Kruse, Sebastian J. Wirkert, Daniel Rahner, Eric W. Pellegrini, Ralf S. Klessen, Lena Maier-Hein, Carsten Rother, and Ullrich Köthe. Analyzing inverse problems with invertible neural networks. *CoRR*, abs/1808.04730, 2018. URL <http://arxiv.org/abs/1808.04730>.
- Yann LeCun, Léon Bottou, Yoshua Bengio, and Patrick Haffner. Gradient-based learning applied to document recognition. *Proceedings of the IEEE*, 86(11):2278–2324, 1998.
- Ziwei Liu, Ping Luo, Xiaogang Wang, and Xiaoou Tang. Deep learning face attributes in the wild. In *Proceedings of International Conference on Computer Vision (ICCV)*, December 2015.

- Kostadin Dabov, Alessandro Foi, Vladimir Katkovnik, and Karen Egiazarian. Image denoising with block-matching and 3d filtering. In *Image Processing: Algorithms and Systems, Neural Networks, and Machine Learning*, volume 6064, page 606414. International Society for Optics and Photonics, 2006.
- Robert Tibshirani. Regression shrinkage and selection via the lasso. *Journal of the Royal Statistical Society: Series B (Methodological)*, 58(1):267–288, 1996.
- Eric Nalisnick, Akihiro Matsukawa, Yee Whye Teh, Dilan Gorur, and Balaji Lakshminarayanan. Do deep generative models know what they don’t know? *arXiv preprint arXiv:1810.09136*, 2018.
- Hyunsun Choi, Eric Jang, and Alexander A Alemi. Waic, but why? generative ensembles for robust anomaly detection. *arXiv preprint arXiv:1810.01392*, 2018.
- Dan Hendrycks and Thomas G Dietterich. Benchmarking neural network robustness to common corruptions and surface variations. *arXiv preprint arXiv:1807.01697*, 2018.
- Eric Nalisnick, Akihiro Matsukawa, Yee Whye Teh, and Balaji Lakshminarayanan. Detecting out-of-distribution inputs to deep generative models using a test for typicality. *arXiv preprint arXiv:1906.02994*, 2019.
- Yoshua Bengio, Nicholas Léonard, and Aaron Courville. Estimating or propagating gradients through stochastic neurons for conditional computation. *arXiv preprint arXiv:1308.3432*, 2013.
- Paul Hand and Vladislav Voroninski. Global guarantees for enforcing deep generative priors by empirical risk. *IEEE Transactions on Information Theory*, 2020.
- Roman Vershynin. Estimation in high dimensions: a geometric perspective. In *Sampling theory, a renaissance*, pages 3–66. Springer, 2015.

A Omitted Proofs

A.1 Proof for Denoising

Proof of Theorem 4.1. We first show that gradient descent with sufficiently small learning rate will converge to $\bar{\mathbf{x}}$, the locally-optimal solution of Equation (10). Recall the loss function $L(\mathbf{x}) := q(\mathbf{x}) + \frac{1}{2\sigma^2} \|\mathbf{x} - \mathbf{y}\|^2$ (we subsume the scaling $\frac{1}{2}$ into $\frac{1}{\sigma^2}$ without loss of generality). Notice in the ball $B_r^d(\mathbf{x}^*) := \{\mathbf{x} \in \mathbb{R}^d \mid \|\mathbf{x} - \mathbf{x}^*\| \leq r\}$, L is $(\mu + \frac{1}{\sigma^2})$ strongly-convex. We next show there is a stationary point $\bar{\mathbf{x}} \in B_r^d(\mathbf{x}^*)$ of $L(\mathbf{x})$.

$$\begin{aligned} \nabla L(\bar{\mathbf{x}}) = 0 &\implies \nabla q(\bar{\mathbf{x}}) + \frac{1}{\sigma^2}(\bar{\mathbf{x}} - \mathbf{y}) = 0 \\ &\implies \nabla q(\bar{\mathbf{x}}) - \nabla q(\mathbf{x}^*) = \frac{1}{\sigma^2}(\mathbf{y} - \bar{\mathbf{x}}) \\ &\implies \langle \nabla q(\bar{\mathbf{x}}) - \nabla q(\mathbf{x}^*), \bar{\mathbf{x}} - \mathbf{x}^* \rangle = \frac{1}{\sigma^2} \langle \mathbf{y} - \bar{\mathbf{x}}, \bar{\mathbf{x}} - \mathbf{x}^* \rangle \end{aligned}$$

From strong convexity of q , $\langle \nabla q(\bar{\mathbf{x}}) - \nabla q(\mathbf{x}^*), \bar{\mathbf{x}} - \mathbf{x}^* \rangle \geq \mu \|\bar{\mathbf{x}} - \mathbf{x}^*\|^2$. Thus

$$\begin{aligned} \frac{1}{\sigma^2} \langle \mathbf{y} - \bar{\mathbf{x}}, \bar{\mathbf{x}} - \mathbf{x}^* \rangle &= \frac{1}{\sigma^2} \langle (\mathbf{y} - \bar{\mathbf{x}}) + (\bar{\mathbf{x}} - \mathbf{x}^*), \bar{\mathbf{x}} - \mathbf{x}^* \rangle \\ &= \frac{1}{\sigma^2} \langle \mathbf{y} - \bar{\mathbf{x}}, \bar{\mathbf{x}} - \mathbf{x}^* \rangle + \frac{1}{\sigma^2} \langle \bar{\mathbf{x}} - \mathbf{x}^*, \bar{\mathbf{x}} - \mathbf{x}^* \rangle \\ &= \langle \nabla q(\bar{\mathbf{x}}) - \nabla q(\mathbf{x}^*), \bar{\mathbf{x}} - \mathbf{x}^* \rangle + \frac{1}{\sigma^2} \|\bar{\mathbf{x}} - \mathbf{x}^*\|^2 \\ &\geq \mu \|\bar{\mathbf{x}} - \mathbf{x}^*\|^2 + \frac{1}{\sigma^2} \|\bar{\mathbf{x}} - \mathbf{x}^*\|^2 \\ &= \left(\mu + \frac{1}{\sigma^2} \right) \|\bar{\mathbf{x}} - \mathbf{x}^*\|^2 \end{aligned}$$

Finally, by Cauchy-Schwartz inequality $\langle \mathbf{y} - \bar{\mathbf{x}}, \bar{\mathbf{x}} - \mathbf{x}^* \rangle \leq \|\mathbf{y} - \bar{\mathbf{x}}\| \cdot \|\bar{\mathbf{x}} - \mathbf{x}^*\|$. So we get $\|\bar{\mathbf{x}} - \mathbf{x}^*\| \leq \frac{1}{1 + \mu\sigma^2} \|\mathbf{y} - \bar{\mathbf{x}}\| \leq \|\delta\| \leq r$, i.e., $\bar{\mathbf{x}} \in B_r^d(\mathbf{x}^*)$. Notice L is $(\mu + \frac{1}{\sigma^2})$ strongly-convex in $B_r^d(\mathbf{x}^*)$, which contains the stationary point $\bar{\mathbf{x}}$. Therefore $\bar{\mathbf{x}}$ is a local minimizer of $L(\mathbf{x})$. Also note that we implicitly require q to be twice differentiable, meaning in a compact set $B_r^d(\mathbf{x}^*)$ its smoothness is upper bounded by a constant M . Thus gradient descent starting from $\mathbf{y} \in B_r^d(\mathbf{x}^*)$ with learning rate smaller than $\frac{1}{M}$ will converge to $\bar{\mathbf{x}}$ without leaving the (convex) set $B_r^d(\mathbf{x}^*)$. \square

A.2 Proof for Compressed sensing

Definition A.1 (Gaussian mean width). *The Gaussian mean width of a set $K \subset \mathbb{R}^d$ is defined as:*

$$w(K) \triangleq \mathbb{E}_{\mathbf{g} \sim \mathcal{N}(0, I_d)} \left[\sup_{\mathbf{x} \in M(K)} |\langle \mathbf{g}, \mathbf{x} \rangle| \right],$$

where $M(K) = \{\mathbf{x} - \mathbf{y} : \mathbf{x}, \mathbf{y} \in K\}$ is the Minkowski sum of K and $-K$.

Intuitively, Gaussian mean width measures the complexity of the set K .

Theorem A.2 (Adapted from Theorem 6.1 by Vershynin [2015]). *Let $K \subset \mathbb{R}^d$ be an arbitrary bounded set, and $A \in \mathbb{R}^{m \times d}$ be a random matrix with its entries sampled iid from Gaussian distribution $\mathcal{N}(0, 1)$, observation $\mathbf{y} = A\mathbf{x}^* + \delta$, where $\frac{1}{\sqrt{m}} \|\delta\|_2 = \epsilon$, and \mathbf{x}^* is unknown. Choose $\hat{\mathbf{x}}$ to be any vector satisfying $\hat{\mathbf{x}} \in K$ and $\frac{1}{\sqrt{m}} \|A\hat{\mathbf{x}} - \mathbf{y}\|_2 \leq \epsilon$. Then*

$$\mathbb{E} \left[\sup_{\hat{\mathbf{x}} \in K} \|\hat{\mathbf{x}} - \mathbf{x}^*\|_2 \right] \leq \sqrt{8\pi} \left(\frac{w(K)}{\sqrt{m}} + \epsilon \right). \quad (13)$$

One consequence of this theorem is that $m = \Theta(w(K)^2)$ measurements are sufficient to guarantee small recovery error.

Remark The statement of Theorem A.2 is only different from the original Theorem 6.1 in Vershynin [2015] where we replaced the ℓ_1 norm assumption by a stronger ℓ_2 norm assumption, and therefore is a slightly weaker version of the original theorem. As indicated in Vershynin [2015], this is still valid. To see this, notice that for any $\hat{\delta} \in \mathbb{R}^m$, we have $\|\hat{\delta}\|_1 \leq \sqrt{m} \|\hat{\delta}\|_2$. So the ℓ_2 bound $\frac{1}{\sqrt{m}} \|\hat{\delta}\|_2 \leq \epsilon$ gives $\frac{1}{m} \|\hat{\delta}\|_1 \leq \frac{1}{\sqrt{m}} \|\hat{\delta}\|_2 \leq \epsilon$.

Theorem A.3 (Restatement of Theorem 4.2). *For a given \mathbf{x}^* and $q = \log p(\mathbf{x}^*)$, define $S(q) = \{\mathbf{x} \mid \log p(\mathbf{x}) \geq q\}$. Recall that the observation for \mathbf{x}^* is $\mathbf{y} = A\mathbf{x}^* + \delta$ where $A \in \mathbb{R}^{m \times d}$ has entries drawn i.i.d. from $\mathcal{N}(0, 1/m)$ and the noise level is $\epsilon = \|\delta\|_2$. When we perform the MAP inference by solving the following problem,*

$$\bar{\mathbf{x}} \leftarrow \arg \min_{\mathbf{x} \in \mathbb{R}^d, \|A\mathbf{x} - \mathbf{y}\|_2 \leq \epsilon} \{-\log p(\mathbf{x})\}, \quad (14)$$

we have:

$$\mathbb{E} \|\bar{\mathbf{x}} - \mathbf{x}^*\|_2 \leq \sqrt{8\pi} \left(\frac{w(S(q))}{\sqrt{m}} + \epsilon \right),$$

where the expectation is over the randomness of A .

Proof. Since $\mathbb{E} \|\bar{\mathbf{x}} - \mathbf{x}^*\|_2 \leq \mathbb{E} \left[\sup_{\mathbf{x} \in S(q)} \|\bar{\mathbf{x}} - \mathbf{x}\|_2 \right]$, the proof directly follows from Theorem A.2 by choosing the set K to be $S(q)$. We only need to verify that $\bar{\mathbf{x}}$ is indeed inside $S(q)$. Notice that both $\bar{\mathbf{x}}$ and \mathbf{x}^* are in the feasible set $\{\mathbf{x} : \|A\mathbf{x} - \mathbf{y}\|_2 \leq \epsilon\}$. Since $\bar{\mathbf{x}}$ maximizes $\log p(\mathbf{x})$ within this set, clearly its density should be at least that of \mathbf{x}^* , i.e. $\log p(\bar{\mathbf{x}}) \geq \log p(\mathbf{x}^*) = q$. Thus $\bar{\mathbf{x}} \in S(q)$.

Note that in our setting the variance of A 's entries is set to be $1/m$ instead of 1 from Theorem A.2. Since the Gaussian mean width $w(S(q))$ is invariant to the scaling of A , we correct the scaling on the noise term and obtain $\mathbb{E} \left[\sup_{\mathbf{x} \in S(q)} \|\bar{\mathbf{x}} - \mathbf{x}^*\|_2 \right] \leq \sqrt{8\pi} \left(\frac{w(S(q))}{\sqrt{m}} + \epsilon \right)$. \square

Remark. Here we show the recovery guarantee when we optimize over the constrained version as in eq. (14). Note that for a suitable constant β , the constrained version $\min_{\mathbf{x} : \|A\mathbf{x} - \mathbf{y}\|_2 \leq \epsilon} \{-\log p(\mathbf{x})\}$ is equivalent to $\min_{\mathbf{x}} \{-\log p(\mathbf{x}) + \beta \|A\mathbf{x} - \mathbf{y}\|_2^2\}$.

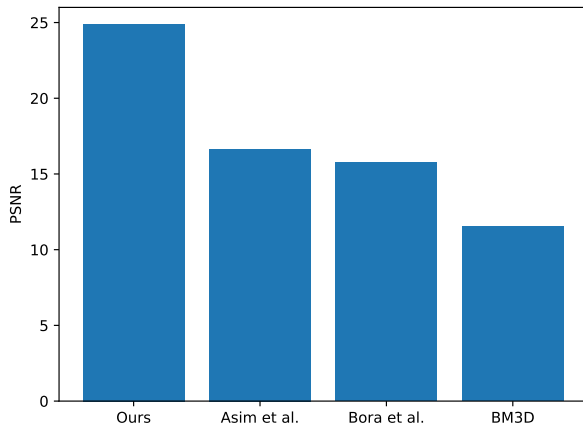
B Additional Experiments and Details

Here we include experimental results and details not included in the main text. Across all the experiments, we used the best hyperparameters for each method.

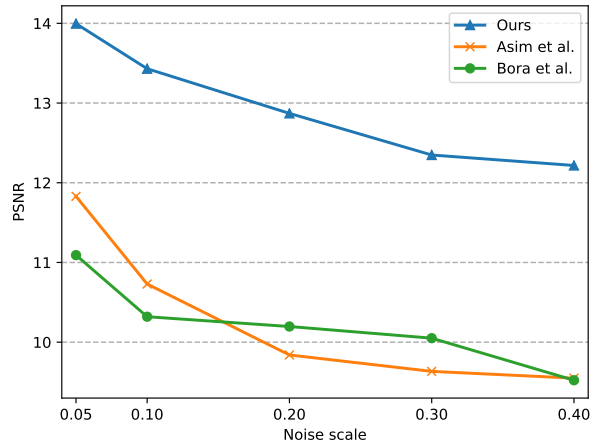
- Ours: Smoothing parameter β chosen from: 0.1, 0.5, 1, 5, 10
 - Bora et al. [2017]: Regularization constant λ chosen from: 0, 0.001, 0.01, 0.1, 1
 - Asim et al. [2019]: Regularization constant γ chosen from: 0, 0.1, 0.5, 1, 5
 - BM3D: Noise variance σ chosen from: 0.1², 0.5², 1, 2², 5² (relative to the maximum noise variance)
- For additional results, please refer to Figures 10a, 10b and 11.

C Model Architecture and Hyperparameters

For the RealNVP models we trained, we used multiscale architecture as in [Dinh et al., 2016], with residual networks and regularized weight normalization on convolutional layers. Following [Kingma and Dhariwal, 2018], we used 5-bit color depth for the CelebA-HQ model. All hyperparameters and samples from the models can be found in Table 1 and Figure 12.



(a) Reconstruction PSNR on the MNIST denoising task.



(b) Result of 1-bit compressed sensing with varying maximum noise scale. Our method achieves far superior reconstruction performance, achieving similar PSNR as [Asim et al., 2019] when the average noise standard deviation is $8\times$ higher, which corresponds to noise power that is $64\times$ stronger.

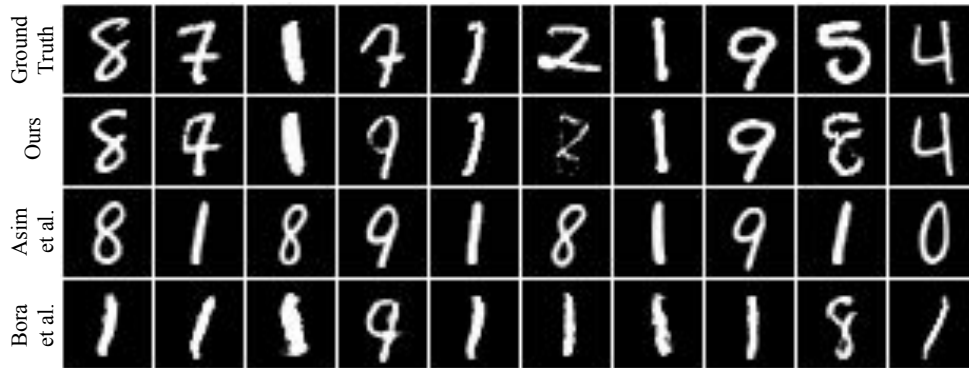


Figure 11: Reconstructions from noisy 1-bit compressive sensing with 3000 binary measurements. Notice that our method fails more gracefully compared to other methods, i.e. even when the reconstructions differ from the ground truth, substantial parts of the reconstructions are still correct. On the other hand, other methods predict a completely different digit. We posit that this is due to our method’s ability to handle non-standard noise.



Figure 12: Samples from the RealNVP models used in our experiments.

Hyperparameter	CelebA-HQ	MNIST
Learning rate	$5e-4$	$1e-3$
Batch size	16	128
Image size	$64 \times 64 \times 3$	$28 \times 28 \times 1$
Pixel depth	5 bits	8 bits
Number of epochs	300	200
Number of scales	6	3
Residual blocks per scale	10	6
Learning rate halved every	60 epochs	40 epochs
Max gradient norm	500	100
Weight normalization regularization	$1e-5$	$5e-5$

Table 1: Hyperparameters used for RealNVP models.